Dynamics of an open elastic rod with intrinsic curvature and twist in a viscous fluid

Sookkyung Lim[a)]
Department of Mathematical Sciences, University of Cincinnati, 839 Old Chem, Cincinnati, Ohio 45221, USA

(Received 13 May 2009; accepted 22 January 2010; published online 23 February 2010)

A twisted elastic rod with intrinsic curvature is considered. We investigate the dynamics of the rod in a viscous incompressible fluid. This fluid is governed by the Navier–Stokes equations and the fluid-rod interaction problem is solved by the generalized immersed boundary method combined with the Kirchhoff rod theory. We classify the equilibrium configurations of an open elastic rod as they depend on the rod's intrinsic characteristics and fluid properties. We assume that the intrinsic curvature and twist are distributed uniformly along the rod. In the case of zero intrinsic curvature (i.e., the stress-free state of the rod is straight), we find a critical value of twist, below which the straight state of the rod is stable. When the twist is above this critical value, however, the rod buckles locally and produces a loop or a plectoneme or a combination of both. When the constant intrinsic curvature is nonzero, we also find a critical value of twist that distinguishes a buckled rod from a stable helix. We also find that fluid viscosity plays an important role in determining equilibrium configuration in this paper. © *2010 American Institute of Physics*.
[doi:10.1063/1.3326075]

I. INTRODUCTION

Filamentous structures that are twisted and bent can be seen in various situations. Examples at small scale include the DNA supercoiling,[1–3] the α-helix in the secondary structure of proteins, and bacteria that swim in an aqueous environment by turning long, thin, helical flagellar filaments.[4–7] Examples at large scale include telephone chords[8] and marine cables. In particular, marine cables under tension and/or torsion on the sea floor form loops and plectonemes (the filament crosses over and under itself repeatedly).[9–11] As a result, there may be mechanical damage and loss of signal transmission. Loops and plectonemes can also be found in small-scale DNA-protein interaction.[2] A common part of the examples above is that those structures are surrounded by a fluid (this fluid has different properties depending on the scale of the fluid-structure interaction problem), and flexibility and torsion of the structure influence its dynamics in fluid. In addition, some filamentous structures undergo a buckling process during loop or plectoneme formation. Therefore, the goal of this paper is to study nonlinear dynamics of an open elastic rod as it depends on the rod's intrinsic characteristics (intrinsic curvature and twist) and fluid properties.

An elastic rod can be a representation of filamentous structures and, therefore, this rod can be represented as a three-dimensional space curve together with an orthonormal triad along the rod with the help of the Kirchhoff rod theory. In the Kirchhoff rod model the space curve represents the centerline of the rod and the triad shows how much the rod bends or twists. The study on the dynamics of an elastic rod *without fluid* has been done for a long time.[12–17] However, the dynamics of an elastic rod interacting *with fluid*, which may provide new features, has not been studied much. In this paper, we will investigate how an elastic rod interacting with a viscous incompressible fluid determines its equilibrium configuration by using the generalized immersed boundary (IB) method. A generalized version of the IB method combined with the nonstandard Kirchhoff rod theory was introduced in Ref. 18 to study the dynamics of a bent, twisted "closed" circular rod in a viscous incompressible fluid. In the generalized IB method there are two important features: [1] the immersed rod applies torque as well as force to the surrounding fluid, and [2] the interaction of the rod with a fluid involves not only translation of the IB points at the local fluid velocity, but also rotation of the associated triads at the local fluid angular velocity. A new aspect of this paper is that we prescribe the intrinsic curvature (stress-free curvature) and intrinsic twist (stress-free twist) distributed uniformly along the elastic rod, i.e., the rod immersed in a fluid is intrinsically curved and intrinsically twisted. One of the advantages of the IB method is that we can ignore rod self-contact. The IB method does not allow the rod to pass through itself because of the continuity of interpolated velocity field.[19–22] There is no need to add artificial conditions to prevent the rod from going through itself unlike other approaches. Therefore, our model can capture the stable loops and plectonemes as postbuckled geometry of the rod without self-contact condition.

In Sec. II, we describe a mathematical model which will be served as an initial configuration in our computational experiments. This model is a perturbation of a straight rod with constant intrinsic curvature and twist. In Sec. III, a mathematical formulation and a numerical scheme will be described based on the generalized IB method together with the nonstandard version of the Kirchhoff rod theory. A rod

[a)]Electronic mail: limsk@math.uc.edu.

initially perturbed will be placed inside of a fluid box and we will see how it deforms into an equilibrium configuration as it depends on control parameters. The control parameters are mainly the intrinsic curvature, the intrinsic twist, and the fluid viscosity. In Sec. IV, we discuss numerical results case by case. The cases include [1] the instability of a straight rod with zero intrinsic curvature and various values of intrinsic twist, [2] helical equilibria concerning nonzero constant intrinsic curvature and various values of intrinsic twist, and [3] nonlinear dynamics of a rod in a fluid with various fluid viscosity values. The simulations for the first two cases will be performed at a fixed fluid viscosity and then we will compare the results with those of the last case study as fluid viscosity varies. The summary and conclusion will be provided in Sec. V.

II. MATHEMATICAL MODEL OF AN ELASTIC ROD

We consider a straight (open and elastic) rod represented by a three-dimensional space curve together with an associated orthonormal triad at each point of the rod. Note that the space curve represents the centerline of the rod and two ends of the open rod are free to move through the fluid. A perturbation of this straight rod with a certain intrinsic curvature and twist will be used as an initial configuration for our computer simulations

Let s be the material coordinate (not necessarily arc length), $0 \le s \le L$, where L is the rest length of the straight rod. Construct a configuration $\mathbf{X}(s)$ and the orthonormal triad, $\mathbf{D}^1(s)$, $\mathbf{D}^2(s)$, and $\mathbf{D}^3(s)$, along the curve as follows:

$$\mathbf{X}(s) = (0,0,(1+\epsilon)s), \tag{1}$$

$$\mathbf{D}^1(s) = (1,0,0), \tag{2}$$

$$\mathbf{D}^2(s) = (0,\cos\epsilon,-\sin\epsilon), \tag{3}$$

$$\mathbf{D}^3(s) = (0,\sin\epsilon,\cos\epsilon), \tag{4}$$

where ϵ is a perturbation parameter.

It is known that the configuration $\mathbf{X}(s)=(0,0,s)$ with an associated orthonormal triad $\{\mathbf{e}_1,\mathbf{e}_2,\mathbf{e}_3\}$ is the equilibrium solution of the classic Kirchhoff rod problem in the absence of the external body forces and moments.[13,14,23,24] Here, $\{\mathbf{e}_1,\mathbf{e}_2,\mathbf{e}_3\}$ is the standard basis in the three-dimensional space. We do not use the equilibrium configuration of the rod because our goal is to study the dynamics of an open elastic rod in a viscous fluid depending on the intrinsic curvature and twist. To do this, we use an initial configuration which is slightly perturbed away from the equilibrium configuration as described above.

III. EQUATIONS OF MOTION AND NUMERICAL METHOD

In this section we state the equations of motion for an elastic rod interacting with a fluid in which the rod is immersed in this fluid. They involve both Eulerian and Lagrangian variables. The Eulerian variables are used to describe the fluid and are defined on the fixed Cartesian coordinate system, and the Lagrangian variables are used to describe the immersed rod and are defined on the moving curvilinear coordinate system. These two types of variables may be interconverted by means of integral transformations that involve a smoothed version of the three-dimensional Dirac delta function.

A fundamental idea of Kirchhoff's theory for thin elastic rods is to describe the forces and moments as cross-sectional averages at each point along the filament. This enables the immersed rod to be represented by a three-dimensional space curve $\mathbf{X}(s,t)$ with an associated orthonormal triad $\{\mathbf{D}^1(s,t),\mathbf{D}^2(s,t),\mathbf{D}^3(s,t)\}$ at each point of the curve, where s is the material coordinate (not necessarily arc length) and t is the time. In the standard Kirchhoff rod model, two constraints are normally imposed on the rod: [1] the rod is inextensible and [2] one of the vectors of the triad (usually $\mathbf{D}^3$) is constrained to be tangent to the space curve. In the IB method, these constraints imply rather complicated boundary conditions in a fluid in which the rod is immersed because of the no-slip condition at the boundary of a viscous fluid. However, we can avoid these conditions on the fluid by allowing the rod to stretch slightly and also by allowing the triad to deviate slightly from the alignment with the tangent direction to the space curve. Instead of imposing the above constraints exactly, we postulate an elastic energy function which tends to maintain them. This energy function will be described later in this section.

The coupled system of equations of the rod and the fluid is as follows:

$$\rho\left(\frac{\partial \mathbf{u}}{\partial t} + \mathbf{u}\cdot\nabla\mathbf{u}\right) = -\nabla p + \mu\nabla^2\mathbf{u} + \mathbf{f}^{\mathrm{b}}, \tag{5}$$

$$\nabla\cdot\mathbf{u} = 0, \tag{6}$$

$$0 = \mathbf{f} + \frac{\partial \mathbf{F}}{\partial s}, \tag{7}$$

$$0 = \mathbf{n} + \frac{\partial \mathbf{N}}{\partial s} + \frac{\partial \mathbf{X}}{\partial s}\times\mathbf{F}, \tag{8}$$

$$\mathbf{F} = F^1\mathbf{D}^1 + F^2\mathbf{D}^2 + F^3\mathbf{D}^3, \tag{9}$$

$$\mathbf{N} = N^1\mathbf{D}^1 + N^2\mathbf{D}^2 + N^3\mathbf{D}^3, \tag{10}$$

$$N^1 = a_1\left(\frac{\partial \mathbf{D}^2}{\partial s}\cdot\mathbf{D}^3 - \kappa_1\right),$$

$$N^2 = a_2\left(\frac{\partial \mathbf{D}^3}{\partial s}\cdot\mathbf{D}^1 - \kappa_2\right), \tag{11}$$

$$N^3 = a_3\left(\frac{\partial \mathbf{D}^1}{\partial s}\cdot\mathbf{D}^2 - \tau\right),$$

$$F^1 = b_1 \mathbf{D}^1 \cdot \frac{\partial \mathbf{X}}{\partial s},$$

$$F^2 = b_2 \mathbf{D}^2 \cdot \frac{\partial \mathbf{X}}{\partial s}, \tag{12}$$

$$F^3 = b_3 \left(\mathbf{D}^3 \cdot \frac{\partial \mathbf{X}}{\partial s} - 1 \right),$$

$$\mathbf{f}^{\mathrm{b}}(\mathbf{x},t) = \int [-\mathbf{f}(s,t)] \delta_c[\mathbf{x} - \mathbf{X}(s,t)] ds + \frac{1}{2} \nabla \times \int [-\mathbf{n}(s,t)] \delta_c[\mathbf{x} - \mathbf{X}(s,t)] ds, \tag{13}$$

$$\frac{\partial \mathbf{X}(s,t)}{\partial t} = \mathbf{U}(s,t) = \int \mathbf{u}(\mathbf{x},t) \delta_c[\mathbf{x} - \mathbf{X}(s,t)] d\mathbf{x}, \tag{14}$$

$$\mathbf{W}(s,t) = \frac{1}{2} \int (\nabla \times \mathbf{u}) \delta_c[\mathbf{x} - \mathbf{X}(s,t)] d\mathbf{x}, \tag{15}$$

$$\frac{\partial \mathbf{D}^i(s,t)}{\partial t} = \mathbf{W}(s,t) \times \mathbf{D}^i(s,t), \quad i = 1,2,3. \tag{16}$$

Equations (5) and (6) are the incompressible Navier–Stokes equations written in Eulerian variables $(\mathbf{x},t)$, where $\mathbf{x}=(x_1,x_2,x_3)$ are fixed Cartesian coordinates and t is the time. The motion of the fluid is subject to the body force $\mathbf{f}^{\mathrm{b}}(\mathbf{x},t)$, which here represents the force per unit volume applied to the fluid by the immersed rod. The vector field $\mathbf{u}(\mathbf{x},t)$ is the fluid velocity and $p(\mathbf{x},t)$ is the fluid pressure. The constant parameters ρ and μ are the fluid density and the fluid viscosity, respectively.

Equilibrium Eqs. (7)–(12) are employed to describe the force and torque of the immersed rod in terms of the space curve and its associated triad, $(\mathbf{X},\mathbf{D}^1,\mathbf{D}^2,\mathbf{D}^3)$. All variables in these equilibrium equations are functions of the material coordinate s and the time t. These are therefore Lagrangian variables. Equations (7) and (8) are balance equations of momentum and angular momentum, respectively.[12,17] The force $\mathbf{F}(s,t)$ and moment (couple) $\mathbf{N}(s,t)$ transmitted across a section of the rod at s can be obtained by averaging the stresses acting across that section. The expressions $-\mathbf{f}(s,t)ds$ and $-\mathbf{n}(s,t)ds$ are the force and torque applied by the arc ds of the rod to the fluid. The internal force and moment on the perpendicular cross section, $\mathbf{F}$, $\mathbf{N}$, and also the applied force density $\mathbf{f}$ and the torque density $\mathbf{n}$ may be expanded in the basis $\{\mathbf{D}^1,\mathbf{D}^2,\mathbf{D}^3\}$, see Eqs. (9) and (10).

Equations (11) and (12) are the constitutive relations of the version of the Kirchhoff rod. The internal moment $\mathbf{N}$ is related to the curvature and torsion through a constitutive law that includes the influence of intrinsic curvature (stress-free curvature) and intrinsic twist (stress-free twist). The component $\mathbf{\Omega}$,

$$\mathbf{\Omega} \equiv (\Omega_1,\Omega_2,\Omega_3) \equiv \left(\frac{d\mathbf{D}^2}{ds} \cdot \mathbf{D}^3, \frac{d\mathbf{D}^3}{ds} \cdot \mathbf{D}^1, \frac{d\mathbf{D}^1}{ds} \cdot \mathbf{D}^2 \right),$$

are the strains of the rod; Ω_1 and Ω_2 are associated with bending, whereas Ω_3 describes physical twist. Here a_1 and a_2 are the bending moduli of the rod about $\mathbf{D}^1$ and $\mathbf{D}^2$, respectively, and a_3 is the twisting modulus of the rod. These moduli are standard in the Kirchhoff rod model.[13] Note that $a_1=a_2$ in the case of a rod with a circular cross section and axially symmetric material properties. The vector (κ_1,κ_2,τ) is called the *intrinsic twist vector*. More specifically, $\kappa = \sqrt{\kappa_1^2+\kappa_2^2}$ is the *intrinsic curvature* and the component τ is the *intrinsic twist* in the stress-free configuration of the rod.[14,23,25] For example, if $(\kappa_1,\kappa_2,\tau)=(0,0,0)$, the rod is said to be *intrinsically straight* and the minimum energy configuration is a straight rod. If $(\kappa_1,\kappa_2,\tau)=(1/r,0,0)$, the rod is said to be *intrinsically circular* and the minimum energy configuration is a ring of radius r. For simplicity it will be assumed here that $\kappa=\kappa_1$ and $\kappa_2=0$, since κ_1 and κ_2 do not matter separately.

The constitutive equations, Eq. (12), are the means by which we approximately enforce the constraints that $s=$arc length and that $\mathbf{D}^3$ should point in the same direction as $\partial\mathbf{X}/\partial s$. The parameters b_1 and b_2 are the shear force constant and b_3 is the stretch force constant. The above unconstrained version of the Kirchhoff rod model can be derived from a variational argument in which we postulate an elastic energy of the form

$$E = \frac{1}{2} \int \left[a_1 \left(\frac{d\mathbf{D}^2}{ds} \cdot \mathbf{D}^3 - \kappa_1 \right)^2 + a_2 \left(\frac{d\mathbf{D}^3}{ds} \cdot \mathbf{D}^1 - \kappa_2 \right)^2 + a_3 \left(\frac{d\mathbf{D}^1}{ds} \cdot \mathbf{D}^2 - \tau \right)^2 + b_1 \left(\mathbf{D}^1 \cdot \frac{d\mathbf{X}}{ds} \right)^2 + b_2 \left(\mathbf{D}^2 \cdot \frac{d\mathbf{X}}{ds} \right)^2 + b_3 \left(\mathbf{D}^3 \cdot \frac{d\mathbf{X}}{ds} - 1 \right)^2 \right] ds, \tag{17}$$

where the first two terms are associated with bending, the third term is associated with twisting, the fourth and fifth terms are related to the shear in the rod, and the last term is related to the extension/compression of the rod. The theory reduces to the standard Kirchhoff rod theory as $b_i \to \infty$ for $i=1,2,3$, see Ref. 18 for more detail.

For simplicity, we assume that $a_1=a_2 \equiv a$, which means the rod is isotropic, and $b_1=b_2 \equiv b$. The bending to torsional stiffness ratio is chosen as $a/a_3=1.5$.

Equations (13)–(15) describe the interactions between the fluid and the rod. These interaction equations connect the Lagrangian and Eulerian variables via a three-dimensional smoothed Dirac delta function $\delta_c(\mathbf{x})=\delta_c(x_1)\delta_c(x_2)\delta_c(x_3)$, which acts as a kernel of the integral transformations that appear in the interaction equations. The particular choice of $\delta_c(\mathbf{x})$ that we make in this work is the following:

$$\delta_c(\mathbf{x}) = \frac{1}{c^3} \phi\left(\frac{x_1}{c}\right) \phi\left(\frac{x_2}{c}\right) \phi\left(\frac{x_3}{c}\right), \tag{18}$$

where $\mathbf{x}=(x_1,x_2,x_3)$ and the function ϕ is given by

$$\phi(r) = \begin{cases} \dfrac{3-2|r|+\sqrt{1+4|r|-4r^2}}{8} & \text{if} \quad |r| \le 1, \\ \dfrac{5-2|r|-\sqrt{-7+12|r|-4r^2}}{8} & \text{if} \quad 1 \le |r| \le 2, \\ 0 & \text{if} \quad |r| \ge 2. \end{cases}$$

Note that $\delta_c(\mathbf{x}-\mathbf{X})$ is a continuous function of $\mathbf{x}$ with continuous first derivatives and with support equal to a cube of edge $4c$ centered on $\mathbf{X}$. Whenever c is an integer multiple of h, the function $\delta_c(\mathbf{x}-\mathbf{X})$ satisfies two identities which hold for all $\mathbf{X}$:

$$\sum_{\mathbf{j}} \delta_c(\mathbf{j}h-\mathbf{X})h^3 = 1, \tag{19}$$

$$\sum_{\mathbf{j}} (\mathbf{j}h-\mathbf{X})\,\delta_c(\mathbf{j}h-\mathbf{X})h^3 = 0, \tag{20}$$

where $\mathbf{j}$ is any vector with integer components, and h is the mesh width of the fluid grid. The above identities ensure that force and torque generated by the rod are correctly applied to the fluid by our numerical scheme. In the original IB method, the mathematical formulation involves the true Dirac delta function. In the present work, however, we need the smoothed approximation from the outset for our formulation which assigns a cross-sectional radius to the space curve that represents the rod. Therefore, c is a physical parameter of the problem which determines the effective radius of the rod.

Equation (14) is the no-slip condition of a viscous fluid, which means that the rod moves at the local fluid velocity. Here, the local fluid velocity is averaged in a manner determined by the smoothed Dirac delta function. Equation (15) states that angular velocity $\mathbf{W}(s,t)$ of the triad associated with the point s of the rod can be obtained as a local average of the angular velocity of the fluid, $(1/2)(\nabla\times\mathbf{u})$. Again, the smoothed delta function is used to determine the appropriate weighted average of the local fluid velocity. We keep track of the orientation of the triad at each point of the rod by the Eq. (16). The triad rotates at the local angular velocity of the fluid and applies torque locally to the fluid.

We discretize Eqs. (5)–(16) both in space and time using the finite difference scheme. The procedure of the numerical method can be summarized as follows: at the beginning of each time step n,

- Compute the auxiliary triad $\mathbf{D}^i_{k+(1/2)}$ at the middle point $s_{k+(1/2)}$ from the triads at s_k and s_{k+1}, where $i=1,2,3$, and k is a point index of the immersed rod.
- Evaluate the internal force $\mathbf{F}_{k+(1/2)}$ and moment $\mathbf{N}_{k+(1/2)}$ transmitted across the section of the rod at $s_{k+(1/2)}$; see Eqs. (9)–(12).
- With $\mathbf{F}_{k+(1/2)}$ and $\mathbf{N}_{k+(1/2)}$ known for all k, compute the applied force $\mathbf{f}_k$ and moment $\mathbf{n}_k$ at s_k; see Eqs. (7) and (8).
- Apply the force $\mathbf{f}_k$ and torque $\mathbf{n}_k$ to the surrounding fluid; see Eq. (13).
- With $\mathbf{u}^n$ and $(\mathbf{f}^b)^n$ known, solve the discretized Navier–Stokes equations for the unknowns $\mathbf{u}^{n+1}$ and p^{n+1} at $(n+1)$ time step using the fast Fourier transform; see Eqs. (5) and (6).
- Move the boundary points at the locally averaged fluid velocity $\mathbf{u}^{n+1}$; see Eq. (14).
- Update the orientation of the triad at each point s_k of the rod; see Eqs. (15) and (16).

TABLE I. Computational and physical parameters.

Parameters	Symbol	Value
Grid size	$N\times N\times N$	$64\times64\times64$
Length of domain		10 cm
Length of rod	L	6 cm
Number of boundary points	n_r	120
Time step	Δt	0.02 s
Fluid density	ρ	1.0 g/cm^3
Fluid viscosity	μ	0.01–100 g/(cm s)
Bending modulus	$a_1=a_2=a$	0.3 g cm^3/s^2
Twist modulus	a_3	0.2 g cm^3/s^2
Shear modulus	$b_1=b_2=b$	54 g cm/s^2
Stretch modulus	$b_3=b$	54 g cm/s^2
Intrinsic curvature	$\kappa=\sqrt{\kappa_1^2+\kappa_2^2}$	0–2.5 cm^{-1}
Intrinsic twist density	τ	$0–4.75\pi$ cm^{-1}
Perturbation	ϵ	0.0001

For a comprehensive description of both mathematical formulation and numerical scheme, the reader is referred to Ref. 18. To test the convergence of the numerical method, calculations were performed for the same physical problem on three different grids, of sizes 64^3, 128^3, and 256^3. Note that in the numerical parameters of the test case the number of points on the rod doubles ($n_r=120$, 240, and 480), and also that the time step Δt is halved ($\Delta t=0.001s$, $\Delta t=0.0005s$, and $\Delta t=0.000\,25s$), for each refinement of the mesh width by a factor of 2. As we refine the computational mesh of the fluid grid, we keep the physical size of the support of the delta function constant by increasing the value of parameter c (δ_{4h}, δ_{8h}, and δ_{16h}). The physical parameter values of the problem were as follows: $\kappa=0.5$, $\tau=0.5\pi$, $\mu=0.01$, and the rest were as shown in Table I. This is a case where the straight rod is unstable and the rod deforms into a stable helix eventually. We first confirmed that the equilibrium configurations of the simulations are independent of grid size and time duration. Then we compared the computed velocity fields at a particular time ($t=0.28s$). Numerical solutions computed on different grids are compared by evaluating the discrete L^2-norm of their difference. The convergence ratios for velocity $\mathbf{u}=(u,v,w)$ in L^2-norm are $\|u_{64}-u_{128}\|_2/\|u_{128}-u_{256}\|_2=1.98$, $\|v_{64}-v_{128}\|_2/\|v_{128}-v_{256}\|_2=2.02$, and $\|w_{64}-w_{128}\|_2/\|w_{128}-w_{256}\|_2=2.28$, which implies that the scheme is first order accurate.

In the IB method, the contact problem is solved automatically. There is no need to add any artificial condition for contact. The reason is that the IB points move in an interpolated velocity field that is continuous and, moreover, has a continuous first derivative. However, the IB method allows

the points to get as close as they like without self-crossing. Their relative velocity does approach zero as they get close.

IV. RESULTS AND DISCUSSION

The stability of a straight rod or a helix may depend on parameters such as the material properties (elastic constants), the intrinsic properties (curvature and torsion), and the geometric parameters (length of the rod and the radius of the rod). In this paper, however, we will focus on the effect of the intrinsic properties to the dynamical response of the rod in a viscous fluid. We therefore fix the constants for the material properties of the rod and the geometric parameters as written in Table I unless otherwise indicated. The control parameters for the fluid-rod interaction problem will be chosen depending on our research interests. In Secs. IV A and IV B we will explore the equilibrium configurations of an open elastic rod in a fluid with a viscosity of $\mu=0.01$ g/(cm s) as the intrinsic twist τ varies while the intrinsic curvature κ is kept fixed at either a zero or nonzero value. In Sec. IV C we will study how the fluid viscosity makes an impact on the deformation of the rod.

Recall that the intrinsic twist vector is $(\kappa_1, \kappa_2, \tau)$, where the intrinsic curvature is given by $\kappa=\sqrt{\kappa_1^2+\kappa_2^2}$ and τ is the intrinsic twist density. It is known that if the intrinsic twist vector is set equal to be a zero vector (we say that the rod is intrinsically straight without torsion), then the initially perturbed rod relaxes toward straight state, that is, the straight rod is stable and is the minimum energy configuration.[17,26] If $\kappa=\sqrt{\kappa_1^2+\kappa_2^2}>0$ and $\tau=0$, the initially straight rod deforms into a circle or a multicovered ring whose radius is equal to $1/\kappa$.[17,23–25]

Note that with a nonzero value of κ, the sign of the intrinsic twist τ determines the handedness of helices. For $\tau>0$, the rod forms a right-handed helix, but for $\tau<0$, the rod forms a left-handed helix. Since the rod is uniform along its length, the energy must remain constant when the sign of τ is reversed. From now on we assume that the intrinsic twist is always positive. By symmetry, numerical results will be same for the negative intrinsic twist.

A. Zero intrinsic curvature and various intrinsic twists

One of the interesting questions in helices is whether a helix is a stable configuration, or an unstable configuration, in other words, whether it deforms into another configuration subject to appropriate boundary conditions. To study this, we compare the numerical results computed with all parameters held fixed other than the intrinsic twist τ. An assumption made here is that the rod is intrinsically straight but twisted, that is, $\kappa=0$ and τ varies. The intrinsic twist density τ will be used as a control parameter. Note that in this section the fluid viscosity is fixed as $\mu=0.01$ g/cm s.

Figure 1 shows a collection of the stable equilibria of an intrinsically straight, but twisted rod with different values of the intrinsic twist τ. The solid line in each panel shows how much the rod twists about its centerline. Note that the unit of the intrinsic twist τ is per centimeter and the length of the rod is the same for each computational experiment. Since the

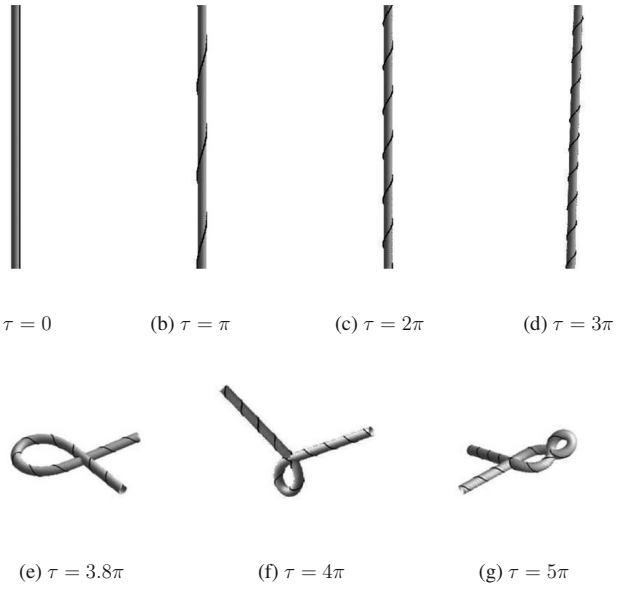

FIG. 1. Equilibria of a twisted straight rod depending on the intrinsic twist τ. Solid line in black along the rod shows the amount of twist. Note: $\tau=\pi$ (per centimeter) implies there are three turns $(=L\times\tau/2\pi)$ along the filament of 6 cm long. Parameters: $a=0.3$, $a_3=0.2$, $b=54$, $\kappa=\sqrt{\kappa_1^2+\kappa_2^2}=0$, and fluid viscosity of water $\mu=0.01$ in centimeter-gram-second (CGS) unit. For the case of (f), the dynamical motion of the rod and time evolution of the elastic energy are shown in Figs. 2 and 3, respectively.

twist density τ is constant along the rod, the total angle of rotation of the upper free end of the rod relative to the lower free end is $\tau\times L$, so the number of turns, q, along the rod can be obtained by

$$q=\frac{\tau\times L}{2\pi}, \tag{21}$$

where L is the length of the filament in centimeter. For example, if $\tau=\pi$ per centimeter and $L=6$ cm are given, then the rod turns three times around the axial curve. Each solid line in Figs. 1(a)–1(d) shows the exact number of turns along the filament at given τ. In our numerical experiments, we found a critical twist τ_c which lies between $3.79\pi<\tau_c<3.80\pi$. For low intrinsic twist $\tau<\tau_c$, the twisted straight rod is stable [see Figs. 1(a)–1(d)], however, for larger intrinsic twist $\tau>\tau_c$, the twisted straight rod becomes unstable and deforms into a helix shortly, and then it shows buckling behavior which is a localized deformation at some points of the rod [see Figs. 1(e)–1(g)]. There is a sudden change when the intrinsic twist reaches a critical value, τ_c, and the straight rod becomes unstable. The geometry just after buckling is a weakly helical shape at short times, as seen in Fig. 2(b). The buckling location lies in the middle of the rod because the two free ends generate no force or moment. As τ increases, buckling behavior occurs in many different points of the rod, or the rod becomes a plectoneme, or the rod becomes a combination of both a loop and a plectoneme for large enough twist. Recall that the IB which represents the centerline of the rod can get as close as it likes without self-crossing.

In the equilibrium configurations, the total energy for the stable straight rods is very low compared to the total energy for the highly deformed rods. The bending energy for the

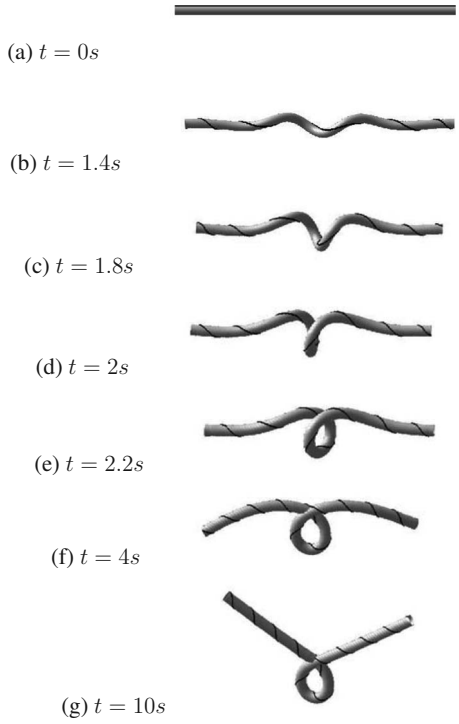

FIG. 2. The time-dependent motion of a rod during buckling corresponding to the case Fig. 1(f). The rod starts out in a perturbed straight rod (a) and deforms into a helix (b) shortly. The frames (c)–(g) show that the rod buckles locally and forms a loop in the middle of the rod. Parameters: $\kappa_1=\kappa_2=0$ and $\tau=4\pi$ in CGS unit.

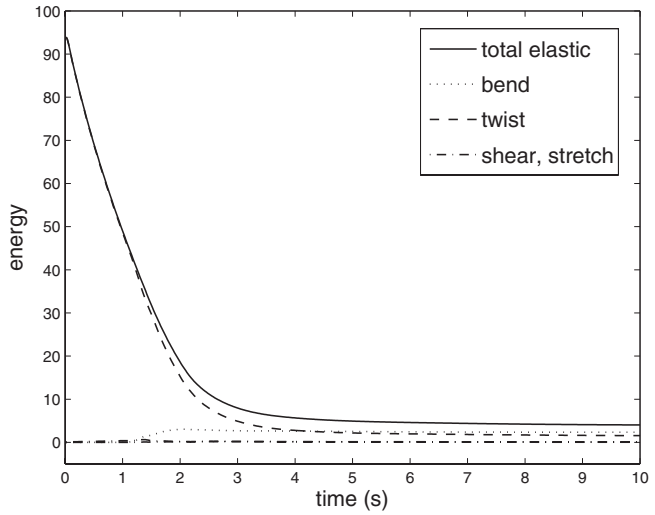

FIG. 3. Time evolution of bend, twist, shear, stretch, and total elastic energy during loop formation. Refer to Fig. 2. Note that shear and stretch energies are negligible.

stable straight, but twisted, rod plays a minor role in comparison to the twisting energy. As τ increases, the rod adopts a loop as a stable state, with the bending energy dominating over the twisting energy. For highly compact form such as a plectoneme, both bending energy and twisting energy (which is lower than the bending energy) play a major role. The values of total energy for the equilibrium configurations in these computational experiments will be reported in Fig. 5 in the following section.

According to the elastic theory[26] for rods, when a rod is subjected to torsion, the critical twist density τ_c in which the straight rod bifurcates is approximately given by

$$\tau_c \simeq 8.98\frac{a}{a_3 L}, \tag{22}$$

where a is the bending modulus, a_3 is the twisting modulus, and L is the length of the rod. Inserting the numerical values (see Table I) used in this work yields the following predicted value for τ_c:

$$\tau_c \simeq (8.98 \times 0.3)/(0.2 \times 6) = 2.245/\text{cm}.$$

There is a discrepancy in the critical twist value between the elastic theory for rods and our model. Note that this analysis was carried without fluid. With fluid, viscous resistance or inertial effect may change the critical value of torsion. We will show how τ_c changes with respect to the change of fluid viscosity in Sec. IV C. Note also that the diameter of the rod is an important factor that affects the critical torsion. It is reported that the diameter of the rod is highly involved in the dynamics of the rod in a viscous fluid.[27] Here we tested how the critical twist is influenced by the diameter of the rod by changing the physical parameter c, where c denotes the order of magnitude of the support of the smoothed delta function δ_c. For the test problem we used $c=4,8$, where the effective radius is proportional to the value of c. Numerical simulations showed that the critical twist decreases with the increase in the effective diameter of the rod. References 28–31 support this observation both theoretically and experimentally. It is reported that for any given lengths of the rod and the values of the elastic constants, the critical amount of torsion, $r\tau_c$, where r is the radius of the rod, is constant without change in the total strain energy. This means that the critical twist τ_c is inversely proportional to the radius of the rod.

According to Eq. (22), for given values of bending and twisting moduli the critical twist density is inversely proportional to the length of the rod. We confirmed that this is also true for our model and the proportionality constant in our model is estimated as 9.3.

Figure 2 shows the evolution in time of an unstable helix in the case of Fig. 1(f). The rod starts out in a perturbed straight, but twisted, rod and takes a form of a helix for a short time, and then the rod buckles locally and forms a loop in the middle of the rod. The loop is formed in the middle by twisting the free ends of the rod because of the boundary conditions in which there is no loading at the free ends. Goriely *et al.*[14,32,33] described this process of loop formation as a sequence of bifurcations of the solutions to the time-dependent Kirchhoff equation for a thin elastic rod in which the twist density is taken as a control parameter. The rod bifurcates three times; first when the twisted straight rod becomes unstable and deforms into a helix, second when the helix becomes unstable, and lastly when the rod forms a loop. Figures 1 and 2 demonstrate that helical rods are unstable when the intrinsic curvature is zero, while the intrinsic twist varies.

Figure 3 shows the time evolution of bend, twist, shear, stretch, and total elastic energies during loop formation

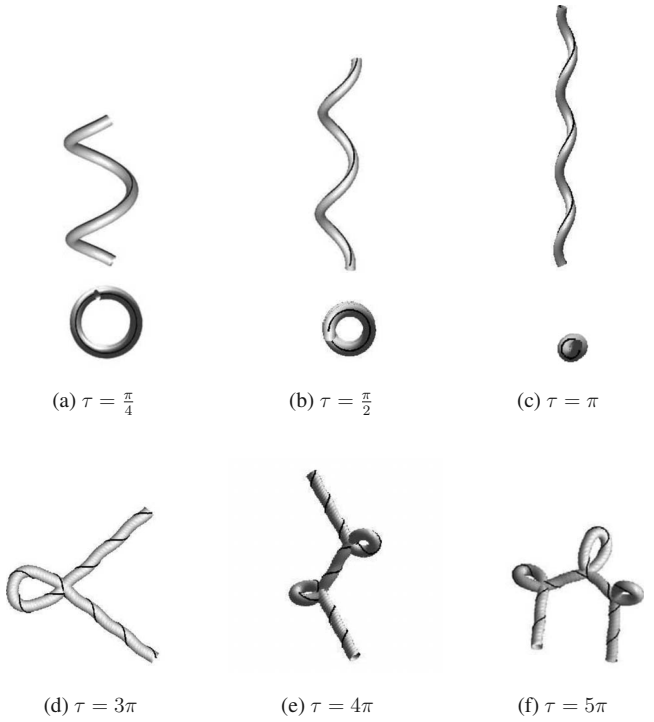

FIG. 4. Helical equilibria for different intrinsic twist τ, while keeping the curvatures $\kappa_1=1.5$, $\kappa_2=0$ per centimeter. Snapshots (a)–(c) show the side views of helices and their projections onto the plane perpendicular to the helical axis. Snapshots (d)–(f) show postbuckled geometries due to high intrinsic twist. There exists a critical twist τ_c near 2.75π that separates unstable from stable helical rods. Parameter values are $a=0.3$, $a_3=0.2$, $b=54$, $\kappa=\sqrt{\kappa_1^2+\kappa_2^2}=1.5$, and fluid viscosity used in these simulations is $\mu=0.01$ in CGS unit.

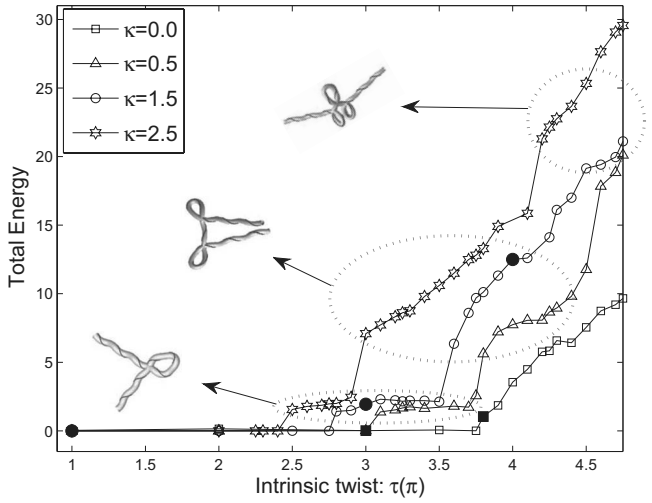

FIG. 5. Total energy for the different intrinsic curvature $\kappa=\sqrt{\kappa_1^2+\kappa_2^2}$ and intrinsic twist τ ranging from π to 4.75π. Configurations corresponding to filled squares (■) are displayed in Figs. 1(d) and 1(e) and configurations corresponding to filled circles (●) are displayed in Figs. 4(c)–4(e). Three configurations shown here are typical forms for some ranges of total energy.

shown in Fig. 2. The bending energy is increasing at the beginning of buckling motion, from $t=1s$ to $t=2s$, which says that torsional strain energy is converted to bending strain energy during buckling process. However, the total elastic energy is monotonically decreasing and converging to a certain value. In our simulations shear and stretch energies are negligible as shown in Fig. 3.

B. Nonzero constant intrinsic curvature and various intrinsic twists

For any given nonzero constant intrinsic curvature, we also found a critical twist that distinguishes from stable helices. When the twist is below the critical twist, the curved, twisted straight rod deforms into a stable helical rod with a certain helical radius and a certain helical wavelength. But for larger twist, the straight rod becomes unstable and forms a helix and then buckles locally at some points of the helical configuration. The final configuration forms a loop or a plectoneme or a combination of both. This implies that a helix becomes unstable as the uniform intrinsic twist of the filament increases.

Figure 4 shows a collection of equilibrium configurations with different intrinsic twist while the curvatures in two directions ($\mathbf{D}^1$ and $\mathbf{D}^2$) are chosen to be $\kappa_1=1.5$ and $\kappa_2=0$ per centimeter, and therefore, the intrinsic curvature is obtained by $\kappa=\sqrt{\kappa_1^2+\kappa_2^2}=1.5$. Our computational experiments indicate that the critical twist lies near 2.75π. For any value of τ less than 2.75π our simulations showed the existence of helices as stable equilibrium configurations, see Figs. 4(a)–4(c). The solid line in each frame shows how much the rod twists around the centerline. As the intrinsic twist τ increases, the helical diameter decreases as appearing in this figure. This means the helix degenerates to a straight rod when the helical radius tends to zero. Figures 4(d)–4(f) illustrate a localized deformation of helical rods for a larger twist. Note that those postbuckled geometries still take the form of a helix with very small helical radius and pitch. The looping process in cases of Figs. 4(d)–4(f) is very similar to a sequence of snapshots in Fig. 2 in which the numerical solutions reveal the dynamic evolution of the rod from a straight state, through an approximate form of a helix, through the dynamic collapse of this helix into a loop with one self-contact point or many self-contact points. This evolution is involved in the dynamic conversion of torsional strain energy to bending strain energy.

Figure 5 shows the total energy of equilibrium configurations with different values of the intrinsic twist that ranges from π to 4.75π. In these experiments we chose four different intrinsic curvatures for comparison which are $\kappa=0$, 0.5, 1.5, and 2.5 per centimeter. When the intrinsic curvature κ becomes larger the bifurcation occurs at a smaller intrinsic twist τ.

In case of zero curvature our simulations showed that both bending and twisting energies of the stable straight twisted rods [see Figs. 1(a)–1(d) and 5 when $\kappa=0$) are approximately zero, which leads to the minimum total energy. However, the total energy is relatively high when the straight rod becomes unstable and goes through large deformation [see Figs. 1(e)–1(g) and 5 when $\kappa=0$]. In case of nonzero curvature stable helices which can be obtained by taking values of intrinsic twist less than the critical value have the minimum energy (close to zero) in comparison to the total energy for loops or plectonemes or complicated geometries.

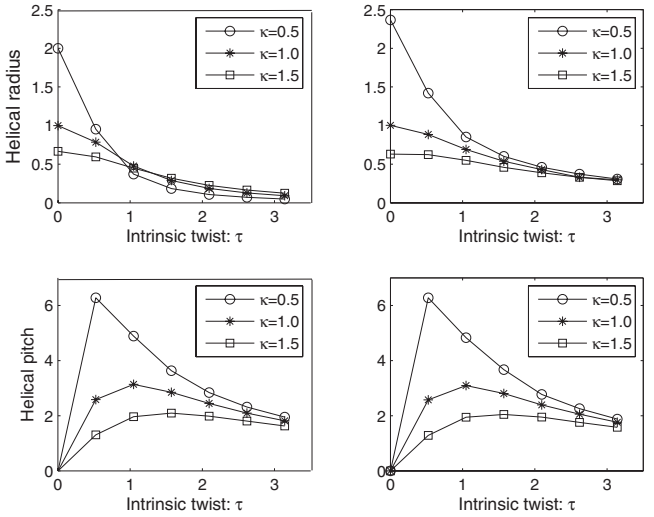

FIG. 6. Left: theoretical values of helical radius (top) and pitch (bottom) of helices based on formula (23). Right: computed values of helical radius (top) and pitch (bottom) of helices formed by our model. τ is the intrinsic twist which ranges from 0 to π and $\kappa=\sqrt{\kappa_1^2+\kappa_2^2}$ is the intrinsic curvature, where $\kappa=0.5$, 1.0, and 1.5. Some helical configurations in the case of $\kappa=1.5$ are shown in Figs. 4(a)–4(c).

For $\kappa>0$, Fig. 5 also illustrates typical equilibrium configurations corresponding to some ranges of the total energy. Notice that the transitions between equilibrium configurations are accompanied by jumps in total energy. When the rod is more compact and highly bent the bending energy is dominating over the twisting energy which plays a minor role.

The constant intrinsic curvature and twist determine the geometry of a helix through the parameters r and p defined as follows:[23,25,34]

$$r=\frac{\kappa}{\kappa^2+\tau^2},\quad p=\frac{\tau}{\kappa^2+\tau^2}, \tag{23}$$

or, equivalently,

$$\kappa=\frac{r}{r^2+p^2},\quad \tau=\frac{p}{r^2+p^2}. \tag{24}$$

The significance of these parameters is that $2\pi r$ is the circumference of the cylinder on which the helix lies, and $2\pi p$ is the axial distance that is traversed during one turn of the helix. These relations imply that the helix degenerates to a straight rod if the radius approaches zero at a constant pitch, and the helix degenerates to a circular rod if the pitch approaches zero at a constant radius, which were also demonstrated by our rod model in a fluid.

Figure 6 illustrates helical radii and pitches of stable helical configurations with three different intrinsic curvatures, where $\kappa=0.5$, 1.0, and 1.5 per centimeter. Two panels on the left display theoretical values of helical radius (top) and pitch (bottom) calculated by formulas (23) and two panels on the right display helical radius (top) and pitch (bottom) of helices obtained by our fluid-rod interaction model. As mentioned before, with zero intrinsic twist the initially straight rod deforms into a circle or a multicovered ring whose pitch is zero. The radii of those configurations are decreasing with increasing curvature (see the top panels in Fig. 6 when $\tau=0$). With nonzero intrinsic twist, the helical radius decreases as the intrinsic twist increases. The computed data shown in Fig. 6 follow similar pattern as the theoretical values but they are slightly higher than the theoretical values. A possible reason for this difference is because our rod is not completely inextensible in which the rod can stretch slightly and its triad can deviate slightly from the tangent vector to the space curve, while the theoretical helix is inextensible and unshearable. Helical radius and pitch computed from the simulations may approach the theoretical values as the stretch modulus and shear modulus $b\to\infty$. An interesting question arisen here is whether or not the helical radius and pitch will be influenced by the change in fluid viscosity. We will discuss this matter at the end of the following section.

C. Dynamics of an elastic rod in a fluid with various viscosity values

The hydrodynamics of large-scale structures such as sea cables is dominated by the inertial force, while the hydrodynamics of small-scale structures such as bacteria is dominated by the viscous force. Recall that the Reynolds number is defined by the ratio of inertial force to viscous force,

$$\mathrm{Re}=\frac{\rho UL}{\mu},$$

where ρ is fluid density, U is the characteristic velocity, L is the characteristic length, and the μ is the fluid viscosity. In our simulations, we evaluated the Reynolds number using a maximum velocity for U (cm/s) and the length of the rod for L (cm). The fluid density is taken to be $\rho=1.0$ g/cm^3. The fluid viscosity is a main control parameter in this section. It appears that as the fluid viscosity μ increases from 0.01 to 100 g/(cm·s), the corresponding flows have Reynolds numbers approximately from 1×10^3 to 1×10^{-3}. The order of magnitude change in Reynolds number is larger than that of magnitude change in fluid viscosity because the peak velocity decreases due to the increase in fluid viscosity.

To study the effect of various fluid viscosity values on the equilibrium configurations of an elastic rod, we first consider one simulation from the previous Sec. IV A which is the case of Fig. 1(f), a loop with one self-contact point, where the intrinsic twist is fixed as $\tau=4\pi$ with zero intrinsic curvature $\kappa=0$. While keeping all parameter values the same as before except for the fluid viscosity, the rod takes the different shape of configuration as μ varies. The left panel in Fig. 7 shows the total energy of the equilibrium configurations as a function of fluid viscosity and displays a couple of typical equilibrium configurations. For $0.01\le\mu<1$, the elastic rod forms a loop with one site of self-contact, but for larger values of fluid viscosity, where $1\le\mu\le100$, the rod forms a plectoneme with two sites of self-contact. Note that the bifurcation may occur at a different value of fluid viscosity by changing other parameters. The right panel of Fig. 7 shows the time evolution of the total energy when μ is assigned the values 0.01, 1, 10, and 100. As observed, the transient time from an unstable twisted straight rod to a

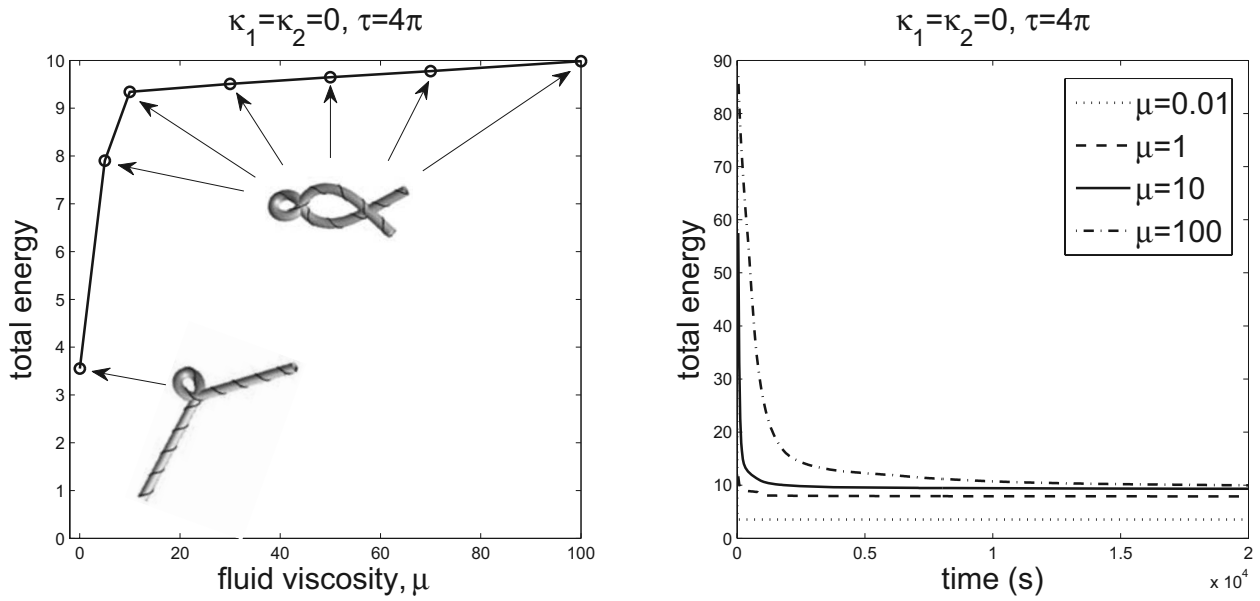

FIG. 7. Left: total energy of the equilibrium configuration vs fluid viscosity. Circles on the left panel correspond to $\mu=0.01,1,10,30,50,70,100$ (g/cm s) in an increasing order. Right: time evolution of total energy for given values of fluid viscosity. Parameter values: the intrinsic curvature is $\kappa=0$ and the intrinsic twist density is $\tau=4\pi$.

stable deformed configuration takes longer for higher fluid viscosity (i.e., for cases of low Reynolds number) in which the rod experiences the viscous drag force as it moves through fluid. It seems that the equilibrium configuration remains the same within some range of fluid viscosity.

Next we explore how fluid viscosity affects the critical twist τ_c when the intrinsic curvature κ is assigned the values of 0, 0.5, 1.5, and 2.5. Simulations were performed to find a critical twist at a given intrinsic curvature and a given fluid viscosity. We observed below the critical twist the perturbed rod relaxes toward a twisted straight rod or a helix as a stable equilibrium configuration, however, the rod deforms into a loop or a plectoneme with self-contact points beyond the critical twist.

Figure 8 shows the relation between the fluid viscosity and the critical twist with four values of the intrinsic curvature. First consider the case where $\kappa=0$. For small fluid viscosity such as $\mu=0.01,0.1$, the rod bifurcates approximately at $\tau_c=3.8\pi$. As μ increases the critical twist decreases with a large difference and then stays at around $\tau_c=3\pi$. Notice that in Fig. 7 the critical value of fluid viscosity that separates a plectoneme from a loop lies between $\mu=0.1$ and $\mu=1$. We also observed that there is a relatively large difference in critical twist between $\mu=0.1$ and $\mu=1$ in Fig. 8. This implies that the critical value of fluid viscosity that separates the low and moderate Reynolds numbers from the high Reynolds numbers lies in the interval of (0.1,1). In fact, $\mu=0.1$ corresponds approximately to the Reynolds number Re=350 and $\mu=1$ corresponds approximately to the Reynolds number Re=10. The Reynolds number decreases radically with the increase in the fluid viscosity. At low and moderate Reynolds numbers the rod is more compact and bent, and it bifurcates sooner in comparison to the high Reynolds numbers as τ increases. In cases of nonzero intrinsic curvatures similar phenomena can be observed, as seen in Fig. 8. Furthermore, at a fixed fluid viscosity the critical twist becomes smaller when the intrinsic curvature becomes larger.

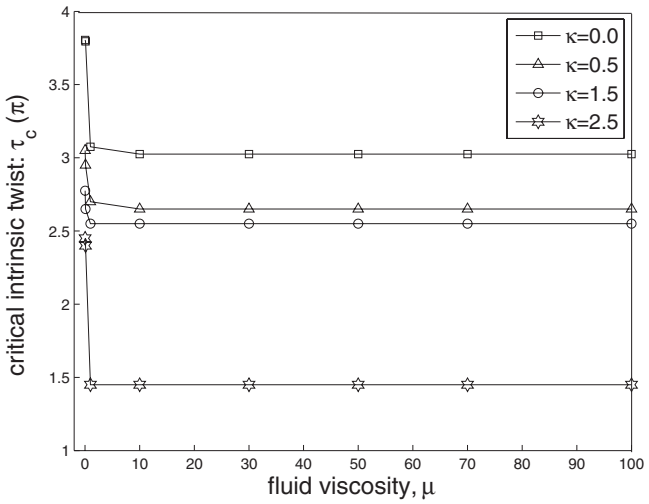

FIG. 8. Critical intrinsic twist density (τ_c) vs fluid viscosity (μ) at four different intrinsic curvatures κ. Indicated points correspond to $\mu=0.01,0.1,1,10,30,50,70,100$ (g/cm s) in an increasing order.

In Sec. IV B we showed that for a certain range of intrinsic curvature and twist the rod forms a helix and its helical radius and pitch depend on the intrinsic properties of the rod. An interesting question arises as follows: do fluid properties affect the helical radius and pitch? Simulations were performed to answer this question in the following way. The intrinsic curvature was taken to be $\kappa=1.0$ throughout these simulations. For any given intrinsic twist chosen from 0 to π we varied the fluid viscosity with a range of $0.01\leq\mu\leq10$. These simulations showed that for any given intrinsic twist the helices retain their helical radii and pitches to within 1%

in spite of various values of the fluid viscosity. From these experiments we can conclude that the helical radius and pitch do not depend on the fluid viscosity.

Throughout this paper we assumed that two ends of the rod are free to move through the fluid. However, we expect that different boundary conditions at the ends of the rod may determine the different shape of the equilibrium configuration of the rod. For example, clamped end conditions tend to produce more stable solutions rather than in a rod with free ends. The instability of an elastic rod with end loading in a viscous fluid will be studied in detail in future work.

V. SUMMARY AND CONCLUSION

The study in this paper extends the dynamics of a circular rod to the dynamics of an open elastic rod in a viscous fluid. We considered an open elastic rod which is intrinsically curved and intrinsically twisted. This rod is immersed in a fluid and this fluid is governed by the incompressible Navier–Stokes equations. Equations of motion which describe the fluid-rod interaction problem are solved by the generalized IB method combined with the nonstandard Kirchhoff rod theory.

We provided classifications of the equilibrium configurations of the open elastic rod depending on the intrinsic characteristics of the rod in which the curvature and twist are distributed uniformly along the rod. When the rod is intrinsically straight we found a critical twist, below which the straight but twisted rod is stable, above which, however, the straight rod becomes unstable and shows the localized deformation, which is the characteristic of buckling behavior. Here, the stable straight rod with small physical twist is the minimum energy configuration. When both intrinsic curvature and twist are set to be nonzero constant, the straight rod becomes unstable and deforms into a helix with a certain radius and a certain pitch for small values of the intrinsic twist. We also found a critical twist, above which the helical rod buckles at some points of the rod. The postbuckled rod keeps the form of a helix. The rod which undergoes a buckling process is arisen from the conversion of torsional strain energy to bending strain energy.

In general, for any given intrinsic curvature, there exists a critical value of twist that separates unstable from stable equilibrium configurations, i.e., straight rods or helices. The stable straight rod is the minimum energy configuration when the intrinsic curvature is a zero value and the stable helical rod is the minimum energy configuration when the intrinsic curvature is a nonzero positive value. Once the rod buckles, the total energy of the final configuration is generally higher as the intrinsic twist increases. When the rod is compact and bent the equilibrium configuration is dominated by the bending energy over the twisting energy.

Fluid viscosity is one of the factors that change the critical torsion with any given intrinsic curvature. For small values of fluid viscosity the rod is less compact and the transition time is very short. But for larger fluid viscosity the rod is more bent and highly compact and the motion of the rod to reach an equilibrium configuration is much slower than that of the rod in a fluid of small viscosity. In the same line the critical twist is higher at lower fluid viscosity. Unlike the critical torsion the helical radii and pitches of helices which occur for nonzero small values of the intrinsic curvature and twist do not depend on the fluid viscosity.

Besides the intrinsic properties of the rod and the fluid viscosity we also observed that the equilibrium configuration of the rod depends on the length of the rod (geometrical parameter) and the ratio of bending modulus to twisting modulus (elastic constants). Changes in those parameter values produce a different bifurcation diagram. For example, the rod with shorter length bifurcates sooner. The study on the instability of open rods with different bending stiffness about $\mathbf{D}^1$ and $\mathbf{D}^2$, which means the rod is anisotropic, may also give rise to an interesting classification of helical equilibria. The effect of the elastic and geometrical properties on the deformation of a rod and the dynamics of an anisotropic rod in a viscous fluid will be left for future work.

ACKNOWLEDGMENTS

The author would like to thank Charles Peskin, David Swigon, and Dong Qian for useful discussions. The author is also indebted to Charles Peskin, David McQueen, and Estarose Wolfson for the use of their visualization software. This work was supported by National Science Foundation Grant No. DMS-0815751.

[1] C. J. Benham, "Onset of writhing in circular elastic polymers," Phys. Rev. A **39**, 2582 (1989).
[2] C. R. Calladine, H. R. Drew, B. F. Luisi, and A. A. Travers, *Understanding DNA: The Molecule and How it Works*, 3rd ed. (Elsevier Academic, San Diego, 2004).
[3] T. Schlick and W. K. Olson, "Trefoil knotting revealed by molecular dynamics of supercoiled DNA," Science **257**, 1110 (1992).
[4] H. C. Berg, "The rotary motor of bacterial flagella," Annu. Rev. Biochem. **72**, 19 (2003).
[5] N. C. Darnton and H. C. Berg, "Force-extension measurements on bacterial flagella: Triggering polymorphic transformations," Biophys. J. **92**, 2230 (2007).
[6] R. M. Macnab, *Escherichia Coli and Salmonella: Cellular and Molecular Biology*, edited by F. C. Neidhardt (Am. Soc. Microbiol., Washington, D.C., 1996), pp. 123–145.
[7] L. Turner, W. S. Ryu, and H. C. Berg, "Real-time imaging of fluorescent flagellar filaments," J. Bacteriol. **182**, 2793 (2000).
[8] E. E. Zajac, "Stability of two planar loop elasticas," Trans. ASME, J. Appl. Mech. **29**, 136 (1962).
[9] J. Coyne, "Analysis of the formation and elimination of loops in twisted cable," IEEE J. Oceanic Eng. **15**, 72 (1990).
[10] C.-L. Lu and N. C. Perkins, "Nonlinear spatial equilibria and stability of cables under uni-axial torque and thrust," ASME Trans. J. Appl. Mech. **61**, 879 (1994).
[11] S. Goyal, N. C. Perkins, and C. L. Lee, "Nonlinear dynamics and loop formation in Kirchhoff rods with implications to the mechanics of DNA and cables," J. Comput. Phys. **209**, 371 (2005).
[12] S. S. Antman, *Nonlinear Problems of Elasticity* (Springer, New York, 1995).
[13] E. H. Dill, "Kirchhoff's theory of rods," Arch. Hist. Exact Sci. **44**, 1 (1992).
[14] A. Goriely and M. Tabor, "The nonlinear dynamics of filaments," Nonlinear Dyn. **21**, 101 (2000).
[15] G. Kirchhoff, "Über das Gleichgewicht und die Bewegung eines unendlich dünnen elastischen stabes," J. Reine Angew. Math. **56**, 285 (1859).
[16] I. Klapper, "Biological applications of the dynamics of twisted elastic rods," J. Comput. Phys. **125**, 325 (1996).
[17] A. E. Love, *A Treatise on the Mathematical Theory of Elasticity* (Cambridge University Press, Cambridge, 1892).
[18] S. Lim, A. Ferent, X. S. Wang, and C. S. Peskin, "Dynamics of a closed

rod with twist and bend in fluid," SIAM J. Sci. Comput. (USA) **31**, 273 (2008).
[19]C. S. Peskin, "Flow patterns around heart valves: A numerical method," J. Comput. Phys. **10**, 252 (1972).
[20]C. S. Peskin, "Numerical analysis of blood flow in the heart," J. Comput. Phys. **25**, 220 (1977).
[21]C. S. Peskin and D. M. McQueen, in *Case Studies in Mathematical Modeling: Ecology, Physiology, and Cell Biology*, edited by H. G. Othmer, F. R. Adler, M. A. Lewis, and J. C. Dallon (Prentice-Hall, Englewood Cliffs, NJ, 1996), pp. 309–337.
[22]C. S. Peskin, *Acta Numerica* (Cambridge University Press, Cambridge, UK, 2002), pp. 1–39.
[23]N. Chouaieb, A. Goriely, and J. H. Maddocks, "Helices," Proc. Natl. Acad. Sci. U.S.A. **103**, 9398 (2006).
[24]A. Goriely and M. Tabor, "Nonlinear dynamics of filaments. II. Nonlinear analysis," Physica D **105**, 45 (1997).
[25]N. Chouaieb and J. H. Maddocks, "Kirchhoff's problem of helical equilibria of uniform rods," J. Elast. **77**, 221 (2004).
[26]L. D. Landua and E. M. Lifshitz, *Theory of Elasticity*, 3rd ed. (Pergamon, Oxford, 1986).
[27]C. W. Wolgemuth, T. R. Powers, and R. E. Goldstein, "Twirling and whirling: Viscous dynamics of rotating elastic filaments," Phys. Rev. Lett. **84**, 1623 (2000).
[28]A. N. Gent and K.-C. Hua, "Torsional instability of stretched rubber cylinders," Int. J. Non-Linear Mech. **39**, 483 (2004).
[29]R. S. Rivlin, "Large elastic deformations of isotropic materials, IV. Further developments of the general theory," Philos. Trans. R. Soc. London, Ser. A **241**, 379 (1948).
[30]R. S. Rivlin and D. W. Saunders, "Large elastic deformations of isotropic materials, VII. Experiments on the deformation of rubber," Philos. Trans. R. Soc. London, Ser. A **243**, 251 (1951).
[31]R. S. Rivlin, in *Rheology, Theory and Applications*, edited by F. R. Eirich (Academic, New York, 1956), Vol. 1, Chap. 10.
[32]A. Goriely and M. Tabor, "Nonlinear dynamics of filaments. III. Instabilities of helical rods," Proc. R. Soc. London, Ser. A **453**, 2583 (1997).
[33]A. Goriely and M. Tabor, "Nonlinear dynamics of filaments. IV. Spontaneous looping of twisted elastic rods," Proc. R. Soc. London, Ser. A **454**, 3183 (1998).
[34]H. Wada and R. R. Netz, "Discrete elastic model for stretching-induced flagellar polymorphs," EPL **82**, 28001 (2008).